A.M. Caporale, A. Airoldi, M. Natali, M. Boiocchi, L. Torre, M. Rallini
Thermomechanical Response of Out-Of-autoclave Infused Carbon-Phenolic Laminates for Rocket Engine Applications Subjected to Surface Ablation
Composites Part A - Applied Science and Manufacturing, Vol. 159, 2022, 107035 (13 pages)
doi:10.1016/j.compositesa.2022.107035

Thermomechanical response of out-of-autoclave infused carbon-phenolic laminates for rocket engine applications subjected to surface ablation

Antonio Maria Caporale[1]*, Alessandro Airoldi *, Maurizio Natali**, Matteo Boiocchi***, Luigi Torre**, Marco Rallini**

*Department of Aerospace Science and Technology, Politecnico di Milano, Via La Masa, 34

20156 Milano, Italy

**University of Perugia, Civil and Environmental Engineering, Strada di Pentima, 4, 05100 Terni, Italy

***Petroceramic S.p.A., Viale Europa, 2, 24040 Stezzano (BG), Italy

[1] Correspondence: antoniomaria.caporale@polimi.it

Keyword:

Carbon Phenolic Composites, Ablatives, Out-of-Autoclave, Thermal Protection System, Heat Transfer Analysis,

Abstract

Cost-affordable and reliable manufacturing technologies to produce Carbon/Phenolic Composites (CPCs) are essential for competitive access to space. These materials are used as ablative Thermal Protection System (TPS) for space applications, such as rocket nozzles or the heat shields of space vehicles. Out-Of-Autoclave (OOA) infusion processes can reduce the manufacturing cost of composites: in this work, OOA produced CPC laminates were compared to Carbon/Epoxy Composites (CECs). The CPCs produced in this work were mechanically characterized to assess their quality and compared with state-of-the-art counterparts through the data available in the open literature. CPC laminates instrumented with ultra-small thermocouples were subjected to Oxy-Acetylene Torch (OAT) ablation testing and a numerical approach was assessed to predict the temperature reached in the laminate layers. Post-burning mechanical tests performed on specimens subjected to the ablation test showed that when the temperature does not exceed a given threshold, the material retains adequate properties to perform a structural role"

1. Introduction

Carbon/Phenolic Composites (CPCs) for high temperature management in space applications have been widely studied in the scientific literature [1-5]. Several studies have been carried out regarding the application of CPCs in the manufacturing and design of rocket nozzles [6-10], which is a crucial field to guarantee a competitive access to space. The major obstacles to this objective are related to the manufacturing and design process of CPC. In fact, in this field, CPCs are exploited as semi-passive Thermal Protection System (TPS) through a surface ablation [4], having at the same time the function of structural material. In charring ablators such as CPCs, a great amount of heat is dissipated by the formation of a solid carbonaceous residue, called char, due to the degradation of the polymer matrix [7]. In general, a good charring ablator should possess high heat capacity and high heat of vaporization [4] and should be able to maintain an adequate residual strength when subjected to severe hyperthermal environments. Typical ex-Polyacrylonitrile (PAN) carbon fibers (CFs) are usually chemically sized to be used with epoxy matrices [11] and CPCs reinforced with ex-PAN CFs are known to have lower mechanical properties than Carbon/Epoxy Composites (CECs), especially in terms of inter-laminar properties and, in general, matrix-dominated properties. Ex-Rayon CFs have been successfully used in the production of CPCs [8, 9] thanks to their characteristic crimped shape, high surface roughness and chemical groups promoting an improved interfacial bond with the phenolic matrix. So, the matrix-dominated properties of ex-Rayon CFs based laminates are from two to four times higher than those of ex-PAN CFs based counterparts, particularly in terms of Inter-Laminar Shear Strength (ILSS) [11]. On the other hand, due to the intrinsic differences between these two types of CFs, the longitudinal tensile strength for ex-PAN CFs based laminates is about four times higher than ex-Rayon CFs based counterparts. Moreover, ex-Rayon CFs have a very limited availability in the market: many suppliers of ex-Rayon CFs have ceased production, also due to the increasingly stringent environmental controls placed upon the discarding of toxic and hazardous by-products of the fabrication process. Accordingly, the possibility to produce CPCs based on ex-PAN CFs exhibiting good interlaminar properties is considered a priority.

The technological process plays a significant role in the production costs, since large CPC-based components for nozzle assemblies are usually produced with autoclave-based processes which are very expensive and do not allow high production volumes. As a result, in some scenarios, the use of

any Out-Of-Autoclave (OOA) process technique to produce some specific CPC parts could promote a certain reduction of the manufacturing time and cost [12].

The characterization and simulation of the ablation process in CPCs was studied in many literatures works [8, 9, 13], and the mechanical properties of the layers that are not directly involved in the ablation process should be carefully investigated, especially considering their temperature dependence [1, 3]. To accomplish such a goal in a relatively simple way, several approaches are available for the numerical analyses of the internal temperature of a composite laminate exposed to high heat fluxes. In particular, a wide literature about the structural polymer-matrix composites subjected to fire have been produced [14-18]. A very interesting approach to study the in-depth degradation processes of composite materials exposed to low heat fluxes (5 W/cm^2) and which can be extended to higher values, has been introduced by Vetter et al. [19]. The protocols introduced in these research works identified the route to estimate the decomposition kinetic parameters and the thermal properties required for any ablation modelling [4, 14-18, 20-22].

The objectives of the present work are related to the production and characterization of CPCs made using an OOA technique and an ex-PAN CF fabric, and to the development of an experimental-numerical protocol to predict both the temperature levels experienced by the structural CPC laminate and the residual strength of the material.

A characterization campaign based on Double Cantilever Beam (DCB) test and +/-45° Tensile test was shaped with the aim to highlight matrix-dominated properties of the produced laminates, and to compare them both with the properties available in open literature [1, 2, 10, 13] and with laminates infused with epoxy resin by using the same technique.

Specifically designed CPC samples equipped with Thermocouples (TCs) were subjected to Oxy-Acetylene Torch (OAT) [23] and then to mechanical characterization of the residual properties based on Four Points Bending (FPB) test and Short Beam Test (SBT). In fact, OAT test was widely used to recreate thermal stresses and heating rates in line with the real environment within a solid rocket motor, as discussed in [4]. At the same time, a finite element thermal analysis was performed and correlated with the experimental data, by adopting a user-defined material law based on one of the models presented in literature [14]. Such a numerical tool makes

possible to correlate the results of mechanical tests with the temperature experienced by the CPC material.

The paper is organized in five sections. After the introduction, the subsequent section is dedicated to the development of the technological manufacturing process. The mechanical characterization of the obtained material is then described in the third section, whilst, in the fourth, the manufacturing of the coupons for the ablation test, the set up of the tests and the development of the thermal numerical approach are described. In the fifth and last section, experimental analysis to achieve a thermal-mechanical correlation is described. Concluding remarks summarize the findings of the research activity.

2. Development of the technological process for the OOA-produced CPCs

The development of CPCs manufacturing process was directly based on an Out-Of-Autoclave (OOA) technique inspired by the work done at NASA Langley Research Centre in 2004 [24]. This technique is referred as Double Bag Vacuum Infusion (DBVI) and relies on a Semi-Permeable Membrane (SPM) that envelopes the laminate inside a vacuum bag. Such a membrane enables the transpiration of the gaseous by-products of the crosslinking reaction of the phenolic resins, but avoid any other leakage, thus enabling the vacuum infusion process. The manufacturing technique was set up to produce woven fabric laminates, with $[0]_{28}$ and $[0]_{8}$ lay-ups, which were used for the characterization of in-plane and out-of-plane properties of the material, described in Section 3. A twill 2x2 ex-PAN CF fabric with an areal density of 200 g/m^2 was used and phenolic resin with a viscosity value close to 400 mPa·s, suitable for infusion process, was selected. Dry CF fabrics were placed on the mold sprayed with a release agent. A layer of peel-ply, one of breather and the SPM were placed onto the CF fabrics in this order and sealed using a high-temperature resistant gum tape to form a first internal bag. The second vacuum bag was made up with a large sheet of the proper plastic material, folded over the mold, previously covered with two layers of breather. A scheme of this setup is showed in Figure 1.

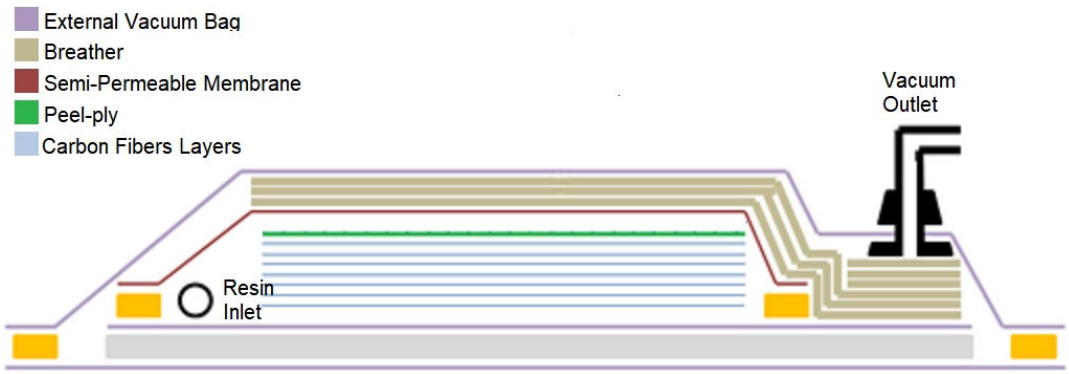

Figure 1. Scheme of Double Bag Vacuum Infusion setup.

The infusion begins as the resin starts to flow inside the vacuum bags. Usually about 85% of the resin is infused in the first 20 minutes. The setup of infusion process is shown in Figure 2-A. Once infusion was completed, resin inlet was closed, and the mold was introduced in an oven to enable the cure of the resin. The vacuum pump was kept turned on to preserve the consolidation pressure. The thermal cycle consisted of three different steps, the first one at 60°C for 80 minutes, the other two at 80°C for 100 minutes and at 150°C for 150 minutes, respectively. Heating rates of 2°C/min were applied during the cycle. Satisfactory results were achieved in most of the trials made with the infusion process, producing laminates with no apparent signs of macroscopic delamination, as it can be observed in Figure 2-B. In other cases, for not predictable reasons, the SPM soaked too much resin i.e., the DBVI-like process did not work properly, inhibiting the consolidation of the composite and leading to slabs with macroscopic delaminations. The analysis of the process outcomes allowed estimating a risk of obstruction of the SPM due to the resin soaked in about 35% of the cases referred to 8 mm thick laminates, which were produced for interlaminar toughness evaluation, described in section 3.1. The production of 2 mm thick laminates presented in Section 3.2 was not affected by such problems. For thick laminates, the risk was mitigated by varying the position of the resin inlet and the vacuum outlet and changing the thickness of the breather indicated in Fig. 1. The final configuration led to obtain good-quality results of the tapered laminates, with a thickness varying from 4 mm to 7 mm, which are described in Section 4.1. The problems and the uncertainties in the setup of the process have to be evaluated considering that phenolics are very difficult to use through vacuum infusion, especially when aimed at producing very thick parts, and in fact, after decades of efforts spent by leading companies and space agencies

such as NASA, this process still presents many criticalities. An analogous procedure was applied to produce $[0]_{28}$ and $[0]_{8}$ lay-up laminates by using an epoxy resin for infusion process (Hexion Epon 862), without the need of using a semi-permeable membrane. In this case, the epoxy resin did not promote any delamination.

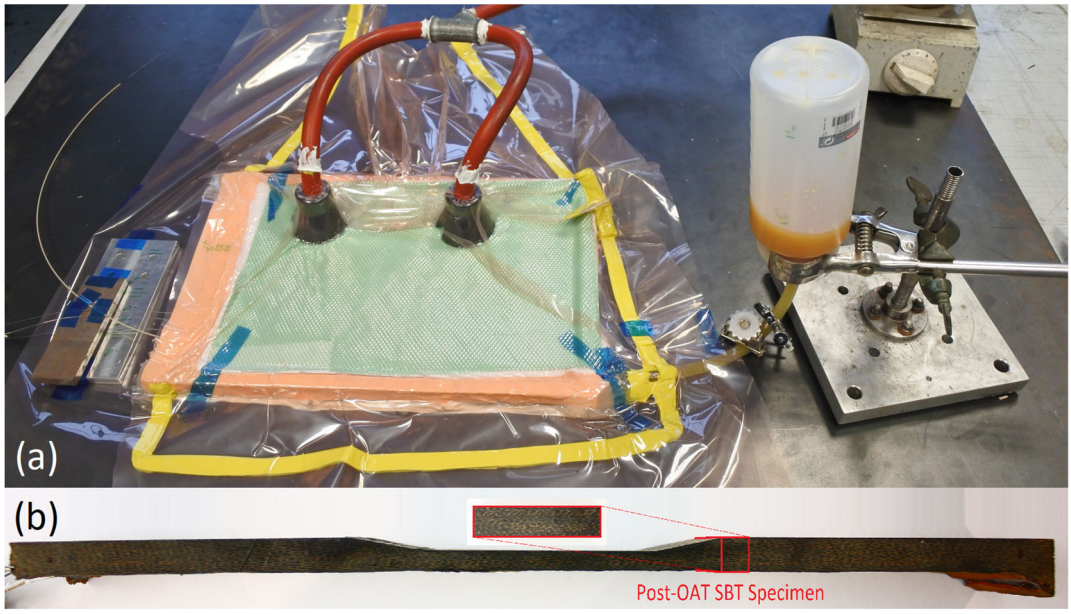

Figure 2. Out-of-Autoclave process: (a) setup of infusion process; (b) detail of a laminate produced.

3. Mechanical characterization

Mode I interlaminar toughness and matrix-dominated properties of the produced laminates were investigated by means of DCB test and+/- 45° Tensile test. The corresponding ASTM standards [25, 26] were used as a guide. An MTS 810 Material Test System was used for all the tests. Results obtained were compared with results obtained by the testing of vacuum infused CECs.

3.1. Double Cantilever Beam Test

The measure of interlaminar toughness is done by recording the crack evolution during the opening of a pre-cracked specimen. It provides an insight on the quality of the produced laminates and on the mechanical properties in the out-of-plane direction, which are typically lower than the corresponding properties in the in-plane direction. Specimens and test were defined following the ASTM D5528 Standard as a guideline [25]. The test was performed on both CPC and CEC specimens.

The pre-crack was obtained by inserting in the mid-plane of the dry stacking sequence a doubly folded sheet of Polytetrafluoroethylene (PTFE), before the infusion.

Three CPC specimens were cut from the $[0]_{28}$ laminate and tested. Their average thickness and width were 7.34 ± 0.05 mm and 25.24 ± 0.04 mm, respectively, while their length was 125 mm. Loads were applied by bonding to the arms of the DCB specimens two hinges, which were then clamped to the test machine, as shown in Figure 3. The MTS 810 system was used to perform a displacement-controlled test at a rate of 0.5 mm/min and a high-definition camera was programmed to acquire a picture every 10 seconds to measure the crack advancement. Following the standard prescription, a crack pre-opening was always performed for all the specimens, to obtain a natural and sharp crack tip from the initial blunt tip originated by PTFE insert. Force-displacement curves are presented in Figure 4-a. Data were elaborated by using the Modified Compliance Calibration (MCC) method, described in the standard [25]. According to such procedure, Mode I inter-laminar toughness G_{IC} was calculated by using Eq. 1:

$$G_{IC} = \frac{3P^2C^{2/3}}{2A_1bh} \tag{1}$$

where P is the measured load, C is the compliance defined as the ratio between the measured displacement and load, b is the specimen width and h is the specimen thickness. A_1 is a characteristic coefficient defined as the slope of the least-square regression of the points obtained by plotting the delamination length, normalized to the specimen thickness, as a function of the cube root of compliance values. Data reduction was performed for several crack lengths to obtain an R-curve, shown in Figure 4-b.

The results of the CPCs were compared with the corresponding data obtained by testing the vacuum infused CEC specimens having a thickness of 7.94 ± 0.04 mm, a width of 20.00 ± 0.06 mm, and the same layup of carbon/phenolic composites. CPC shows an average toughness of about 307.8 ± 27.1 J/m^2, which is lower than CEC case. Such toughness values are not very high for a composite fabric, but are adequate for aeronautical grade composites, considering that unidirectional carbon-epoxy reinforced AS4-8552 have mode I toughness lower than 300 kJ/m^2 [27, 28]. The chemical compatibility of phenolic resin and common ex-PAN carbon fibers is lower than the one referred to epoxy resin, so that the comparison with CEC laminates, which

exhibit a toughness 29% circa higher can be considered a positive result. Higher values are reported in literature for mode I toughness of composite produced by infusion process with phenolic resin, but they are referred to different processes or to different types of carbon fibers [4, 30-32].

It is also worth noting that the test repeatability and the constant values obtained for G_{IC} with the crack length, both for CPC and CEC laminates, indicate the absence of macroscopic defects in the thick $[0]_{28}$ laminates produced and confirm the possibility to manufacture CPC laminates by using DBVI-like techniques and ex-PAN carbon fibers with acceptable inter-laminar properties.

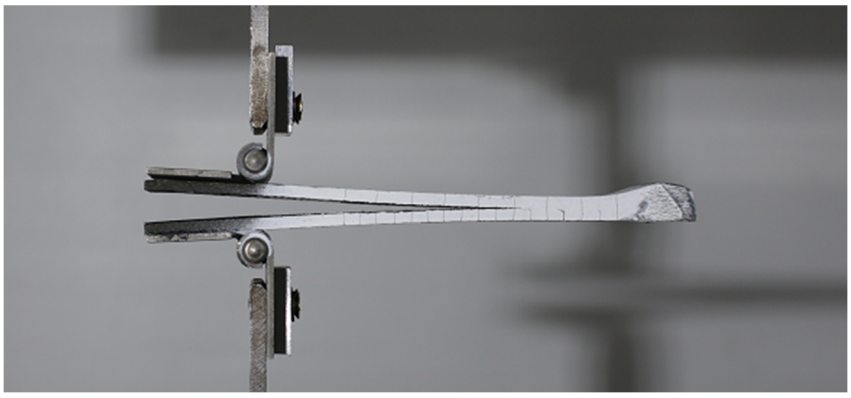

Figure 3. Example of a specimen for DCB test.

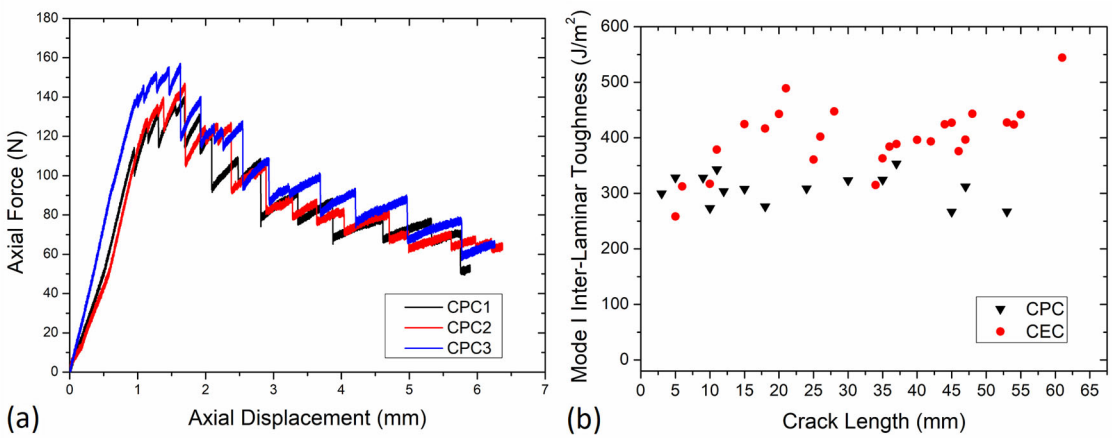

Figure 4. (a) DCB Force/Displacement curves; (b) Mode I Inter-Laminar Toughness compared with infused Carbon/Epoxy.

3.2. Tensile test on +/-45° laminates

The matrix-dominated properties in the plane of the plies were assessed by accomplishing tests on $[45]_8$ cut from $[0]_8$ fabric laminates produced with the OOA technique. ASTM D3518 Standard was used as guideline [34]. Tensile test of a +/-45° composite laminate causes a matrix-dominated response with damage and failure mainly induced by Intralaminar Shear Stress state. Two CPC specimens and four infused CEC specimens were tested; Specimens measures are reported in Table 1:

Table 1. +/-45° tensile specimen measures

Specimen	***Thickness***	***Width***	***Length***
	mm	mm	mm
CPC	1.9 ± 0.02	25.27 ± 0.08	200
CEC	2.06 ± 0.08	25 ± 0.05	200

Tapered tabs made of E-Glass/Epoxy laminates were applied at the ends of the specimens. A displacement-controlled tests, at a rate of 0.75 mm/min, was performed by using the MTS 810 system. Results in Figure 5 show that, if CECs have a significantly higher strength and toughness, CPCs and CECs show a similar behavior in the elastic range. This confirms that in the cases in which the OOA process did not exhibited technical problems during the manufacturing, the technique adopted did not have a detrimental effect on the matrix-dominated in-plane properties of the CPCs.

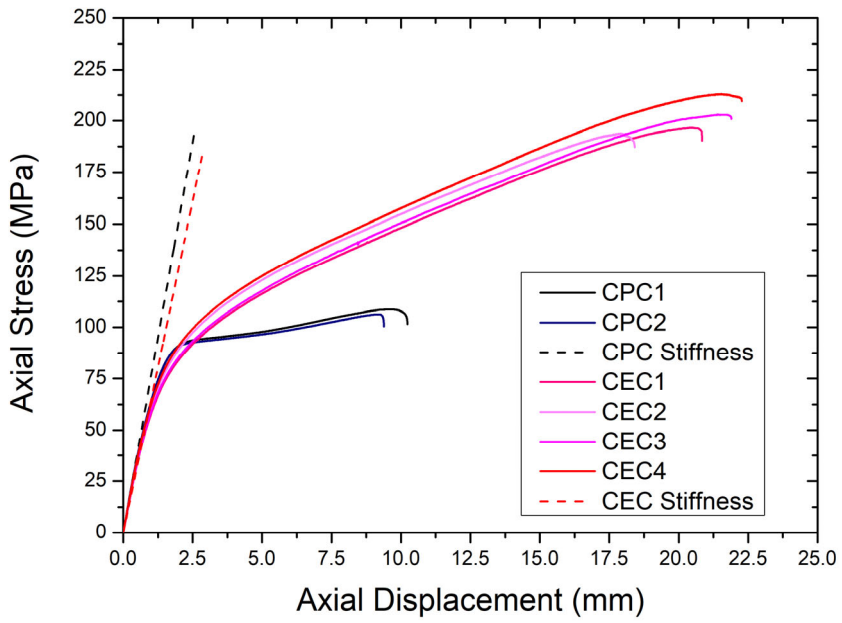

Figure 5. Stress/displacement curves of +/-45° tensile tests CPC and CEC.

4. Ablation test and numerical modelling

A testing campaign based on an OAT was carried out to characterize the ablation response of the produced CPCs. Indeed, OAT is the most common and affordable way to perform a test which can partially simulate the severe hyperthermal environment of a rocket [4]. The OAT is generally able to produce a high temperature flame (up to approximately 3000°C) and a heat flux up to ~ 900 W/cm^2 [4, 33] ASTM-E-285-80 provides the general guidelines to arrange a test bed based on an oxy-acetylene torch. The OAT is calibrated through a copper slug calorimeter according to ASTM-E457-08 [34]. The OAT specimens were designed to have a network of thermocouples embedded inside, as temperature monitors. In this way, the temperature data were used to validate a numerical approach for the prediction of temperature in the internal layer during the tests.

4.1. Tapered specimen design and production

A tapered coupon was designed for the OAT ablation test and the subsequent mechanical testing. The identified shape (Figure 6-a) meets the following four criteria:

I. the specimens had to be thick enough to be representative of nozzle walls and to present measurable residual strength after the exposure to OAT;

II. since thermocouples should be placed at different locations, to validate a thermal model for the prediction of temperatures, their introduction would have negatively affected the local mechanical properties in the regions where sensors were inserted. Accordingly, the TCs were located in a zone where they did not relevantly influence the strength in the mechanical tests following the exposure to OAT;

III. the specimen's failure in the mechanical tests following the OAT test should have been influenced both by in-plane and out-of-plane material properties [36-39];

IV. considering that through an ad-hoc designed sample holder the torch plume impinged only in the red areas highlighted in Figure 6-b, the tapered coupons reported in Figure 6-b had to be sized to allow the characterization of the residual mechanical properties through FPB and SBT tests.

In the thick part, the specimen was produced with a lamination sequence of $[0]_{28}$ of woven fabric and an average thickness of 7.90 ± 0.35 mm. In the thin part, it has a lamination sequence of $[0]_{16}$ of woven fabric and a thickness of 4.59 ± 0.23 mm. The average width is 40.82 ± 0.59 mm, and the length is 280 mm. The tapering was obtained by stacking up sixteen 280 mm long plies and, dispersed among them, twelve short plies per side were placed to create the taperings. The length of these plies ranges from 110 mm at the base of the tapering to 92 mm at the top of the tapering.

The oxy-acetylene torch was applied on the surfaces of the thick ends (red zones in Figure 7-b), at the beginning of the tapering, so that the heat flux could promote a reduction of mechanical properties both in the thick parts and in the tapered section, potentially inducing a degradation of the matrix and mechanical properties also in the expected failure zone. Moreover, even though the torch was applied in both red areas of the sample (as reported in Figure 7-b), thermocouples were inserted in only one of the thick sides, to measure the internal temperature and to provide data to calibrate a numerical model, with a minimal influence on the mechanical strength of the weakest section. Finally, the width of the specimen was set to 40 mm, which was adequate to carry out the characterization of the residual properties. In fact, specimens were designed to both be tested in FPB or to be cut to obtain SBT samples.

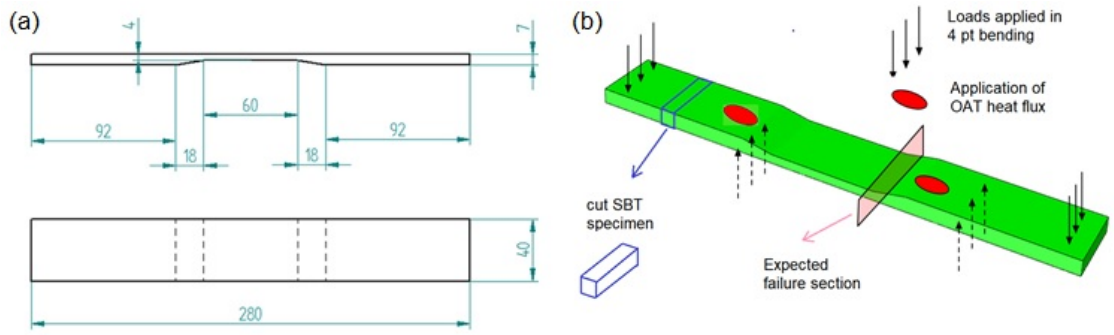

Figure 6. Tapered Specimen: (a) design with measure in mm and (b) scheme of oxy-acetylene torch and Four Points Bending (FPB) tests, including the possibility to cut SBT specimens.

The tapered specimens were produced by adopting minor changes in the same double bag vacuum infusion (DBVI) technique presented in Section 2 (24). Specifically, a mold shaped for tapered specimens was used and three Tersid Type K TCs with a diameter of 0.5 mm were embedded in some of the specimens produced, at one of the thick ends. Each infusion process made possible the production of three/four specimens. The scheme of the temperature sensing system is presented in Figure 7. Three thermocouples were embedded in each sample: TC1 was placed at the beginning of the tapered zone, between the sixth and the seventh layer from the top (approximately 1.70 mm from the surface), while both TC2 and TC3 were placed between the thirteenth and fourteenth layer from the top (approximately at 3.64 mm from the surface), with the Seebeck junction positioned towards the end of the tapering zone and closer to the lateral side of the specimen.

To this purpose, an additional dam constituted by silicone strips was sealed with the inner bag of the DBVI configuration. In this way, the TCs were protected at the inlet from potentially dangerous stress levels induced by the consolidation pressure, maintaining the sealing and avoiding leakages during infusion and curing. The production of tapered specimens with a more complex geometry of a flat laminate, represented a further development of the original DBVI technique (24).

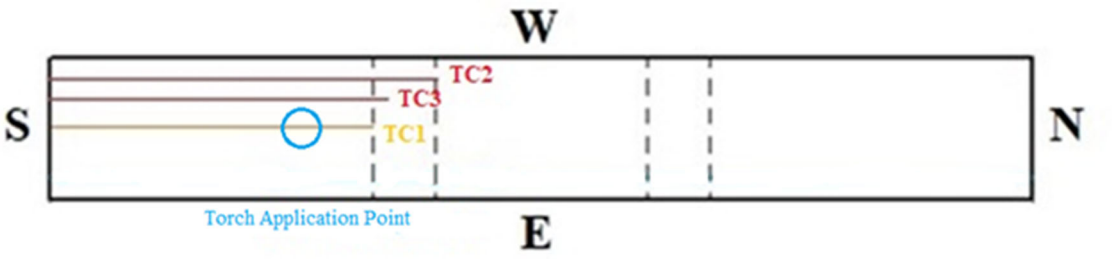

Figure 7. Thermocouples Network inside a tapered specimen.

4.2. OAT ablation test setup

A sample holder, shown in Figure 8-a was used to integrate the tapered coupon in the OAT test bed and to control the experimental conditions. The holder was made of high temperature steel and was characterized by a wall with a thickness of 5 mm, featured with an 8 mm diameter hole (Figure 8-a), with the function to accurately control the area directly exposed to the torch plume, enabling a correct reconstruction of the boundary conditions in the numerical models (Figure 6-b). The tapered coupon was maintained in position by a set of screws acting on the back flat surface, while the tapered surface was forced to stay in contact with the inner surface of the sample holder avoiding the leakage of the combustion gases on other areas of the sample (Figure 8-b). Ideally, the torch plume should act only on the 8 mm circular area delimited by the hole in the sample holder.

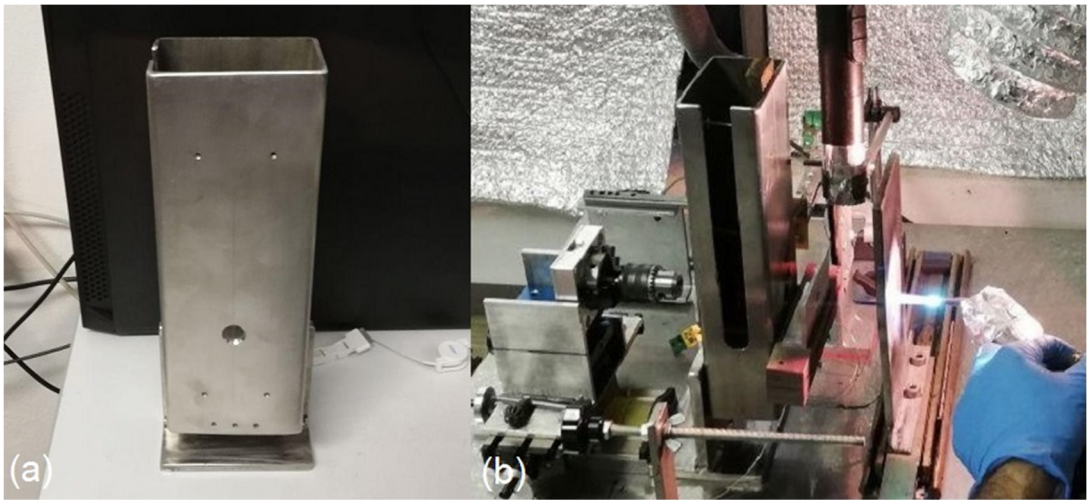

Figure 8. OAT test: (a) Sample holder, (b) accomplishment of the test.

The mixture of oxygen and acetylene was regulated to achieve a nominal heat flux of 800 W/cm^2 and a neutral flame. Several coupons were tested to assess and calibrate the test procedure. As reported previously, the torch plume was applied on both sides of the coupon in the red areas reported in Figure 6-b. More precisely, each test article was tested twice to increase the number of experimental points. After a first test on one side of the coupon we re-used this sample and then carried out an additional test on the other side of the same test article. The repeatability of testing conditions was difficult to be achieved, due to the development of the ablation crater which made possible the penetration of gases inside the holder, thus modifying the area where the flow was directly applied.

In a final testing phase, a duration of 30 s was adopted for each shot. In these tests, a crater was formed with a typical depth of about 1 mm per shot. A sampling frequency of 100 Hz was used to acquire the temperature profiles of the three TCs embedded in the coupon. Starting from these final testing conditions, two tests, performed on the sides equipped with the thermocouples were selected to provide the data for the development and calibration of the numerical model.

4.3.Numerical Approach for the analysis of internal temperature in CPC laminate subjected to ablation

Although modelling of ablation phenomena involves complex multi-physics analyses, simple approaches can be used, particularly if the objective is the evaluation of temperature experienced by the internal layers of a laminate that is subjected to an ablation process on the surface. Indeed, there is a wide literature about the structural polymer-matrix composites subjected to fire [14-18], which can be adopted as a guideline to develop a procedure that could be implemented in a multi-purpose Finite Elements code, available at the commercial level for design and analysis. Among the available methods, Lattimer et al. presented a simplified model [14], where the degradation of the material is described through the variation of density, which decreases due to the chemical reactions and phase transformations. In the model, independency of heating rate is postulated. Accordingly, the density is a function of the maximum temperature reached by the material, under the model assumptions: $\rho = \rho(T_{max})$. A unidimensional problem is hereby considered to describe

the approach where transformation reactions take place on the surface of an element and x is the thickness direction. The assumptions of the model lead to an energy balance written as in Eq. 2.

$$\left[\rho C + Q\frac{\partial \rho}{\partial T}\right]\frac{\partial T}{\partial t} + \dot{m}_g'' C_g \frac{\partial T}{\partial x} = \frac{\partial}{\partial x}\left(k\frac{\partial T}{\partial x}\right) \quad (2)$$

where ρ is the instantaneous density, C and k are the specific heat and the conductivity of the material, respectively, Q is the degradation heat, T is the temperature, $\dot{m}_g''$ is the first time-derivative and second space-derivative of mass of gaseous fuel within the void volumes , C_g their specific heat and x is the spatial coordinate [14]. The enthalpy related to the energetic cost of the degradation endothermic reactions can be added to the specific heat to form a single term, defined as apparent specific heat (Eq. 3).

$$\rho_v C_{app} = \left[\rho C + Q\frac{\partial \rho}{\partial T}\right] \quad (3)$$

The second term of Eq. 2 is the heat loss due to the convection of gases. The results presented in [14] indicate that this term can be neglected, so that, eventually, Eq. 2 can be considered a thermal energy balance of a material with a specific heat C_{app} and a conductivity k.

The application of Eq. 3 makes possible the evaluation of the apparent specific heat once that the curve $\rho = \rho(T)$ and its derivative, specific heat C, and degradation heat Q are known.

The change of material composition also affects the thermal conductivity and the specific heat. Therefore, both these properties can be related to the density through a rule of mixture that combines the properties of the original material with the ones of the charred material. For the implementation of this rule of mixture, it is convenient to describe the progression of degradation through a density scale factor, defined as in Eq. 4.

$$F(T) = \left[\frac{\rho(T) - \rho_d}{\rho_v - \rho_d}\right] \; with \; F(T) \in [0,1] \quad (4)$$

where the two subscripts d and v stand for "*degraded*" and "*virgin*", respectively, and virgin means non-degraded. By definition, F ranges from 1 (completely virgin) to 0 (completely degraded). The scale factor is used to express the rule of mixture that provides the conductivity, k, and the specific heat, C, as a function of temperature (Eq. 5 and 6):

$$k(T) = Fk_v + (1 - F)k_d \quad (5)$$

$$C(T) = FC_v + (1 - F)C_d \quad (6)$$

According to this mono-dimensional approach, an equivalent material can be introduced in a standard finite element code to solve a generic three-dimensional problem of heat transfer. The thermal response of the material will be characterized by the apparent specific heat, C_{app}, thermal conductivity, k, and specific heat, C. All these parameters will vary with temperature as expressed in Eq. 4, 5 and 6.

The approach was implemented in the Simulia/Abaqus Standard code to simulate the temperature in the internal layer of the laminate during the OAT tests.

The calibration of the model required a density vs temperature curve, which can be obtained experimentally, and the values of degradation heat Q.

Actually, the irreversibility of the degradation process must be taken into account, avoiding that the heat adsorbed in the process could be returned when temperature decreases. The introduction of the irreversibility required the definition of an ad-hoc material model, which was implemented in a UMATHT subroutine linked to the Simulia/Abaqus Standard code. The subroutine was written to define all the properties for a generic thermally orthotropic material. The function of the subroutine is the evaluation of the heat fluxes and the internal energy variation given the temperature, with properties that are assessed by distinguishing three cases:

I. temperature is growing, and it is above T_{max} , which is the maximum temperature reached in the simulation history: in this case the material is degrading, and the degradation heat contribute shall be included in the specific heat;
II. temperature is growing, but it is below T_{max}: in this case the material is heating, but it has been already degraded beyond the level corresponding at the current temperature, so that the degradation heat contribution shall not be included;
III. temperature is decreasing: in this case the degradation heat contribute shall not be included in the specific heat.

The implementation of this model into Simulia/Abaqus was verified by simulating the validation test described in [14]. This test involved a Glass/Vinyl-Ester composite plate subjected to a heat flux on one side and was modelled in [14] by using a mono-dimensional finite difference approach, implementing Eq. 2. A model of the test was developed by using Simulia/Abaqus code, including the UMATHT that implements the material model described above. The finite element model is shown in Figure 9-a. The comparison between the numerical results presented in [14] and the corresponding obtained with the Simulia/Abaqus model developed in this work are presented in Figure 9-b. Considering the differences in the numerical approaches and that the finite element model is three-dimensional, while the one presented in [14] was performed by using a mono-dimensional version of the model, the two simulations provide similar results.

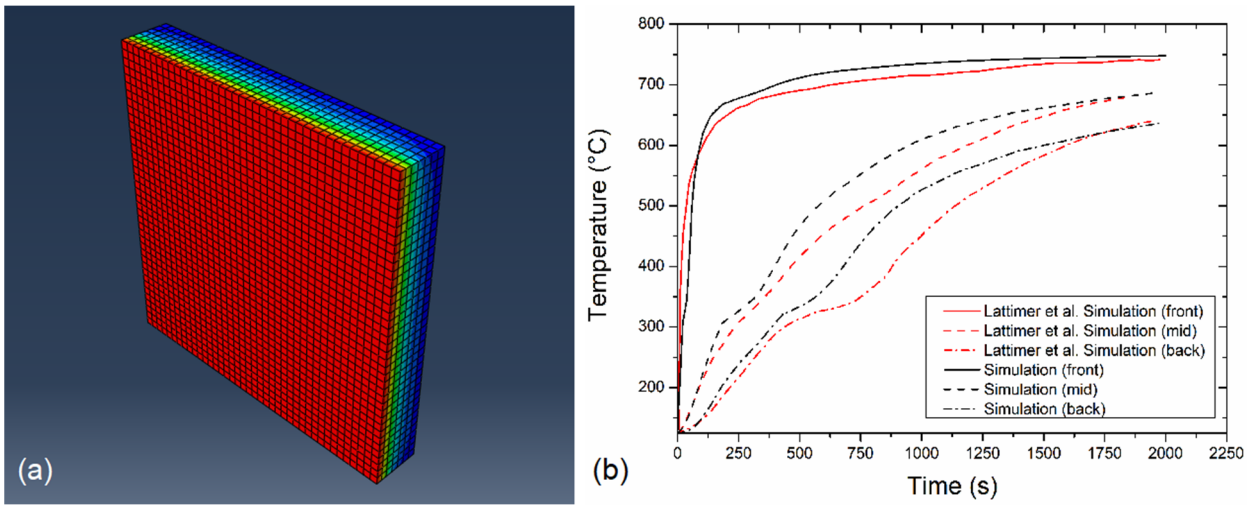

Figure 9. Verification of Lattimer et al. model: (a) FEM model, (b) comparison between temperatures simulated in this work and in [14].

4.4. Simulation of the ablation test

Once the approach for the numerical thermal model was set up and verified, it was applied to simulate the temperature profile during the oxy-acetylene torch ablation tests. The geometry of the tapered specimen was represented by using a mesh of solid elements Type DC3D8 shown in Figure 10-a, with a typical size of 1 mm in the thickness and 2 mm in the other dimensions. Eight and four elements were used in the through-the-thickness direction in the thick and thin part of the specimen, respectively. Three boundary conditions have been set up:

I. a surface heat flux with the same power of the oxy-acetylene torch used in the ablation test, localized in the circular area of application of the torch;

II. thermal radiation from all the surfaces of the specimen, using Stefan-Boltzmann equation for grey bodies; sink temperature was chosen to be the average of the of the temperature inside the sample holder during the test.

III. surface film condition to simulate free convective flows; the same sink temperature used for thermal radiation was used also here and the film coefficient was calculated with the theory of isothermal vertical plate natural convection $h = Nu \cdot k/H$, where h is the film coefficient, Nu is the Nusselt number, k is the thermal conductivity of air at the sink temperature defined, and H is the height of the plate.

The parameters related to the boundary conditions are summarized in Table 2. Density function $\rho = \rho(T)$ (in Figure 10-b), virgin specific heat C_v, virgin Out-of-Plane thermal conductivity k_v^{OOP} were obtained experimentally. In particular, the density of the material was obtained through thermo-gravimetric analysis TGA. The tests were performed in nitrogen with a thermo-gravimetric analyzer (Seiko Exstar 6300); dynamic scans were performed at a heating rate of 20 °C/min from room temperature up to 1000 °C. To obtain a good reproducibility, at least 3 samples for each material were tested. Powdered samples of about (10 ± 1) mg were used for each material. Moreover, thermal conductivity tests were performed in nitrogen using a Netzsch LFA 457 Microflash testing machine, implementing the ASTM E-1461 and DIN EN 821 Standards, from room temperature up to 800°C.The values for the other material properties were defined considering the data published in open literature for CPCs [1-3, 10, 13, 40, 41]. The set of material parameters chosen is presented in Table 3.

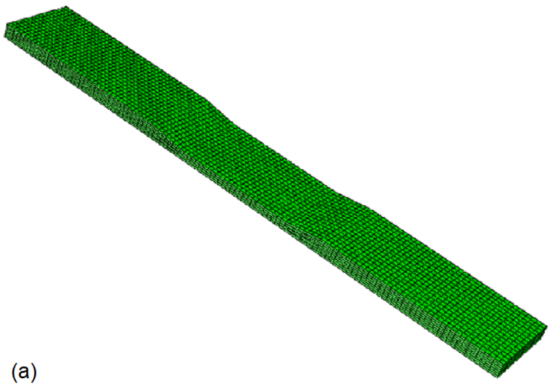

(a)

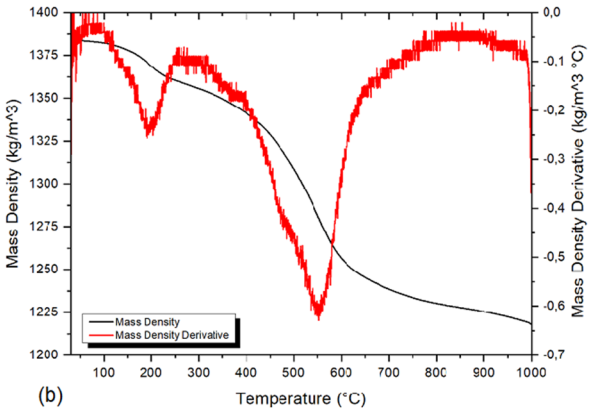

(b)

Figure 10. Modelling of ablation tests: (a) finite element mesh, (b) mass density curve with temperature and its derivative. Vertical lines show the three steps of degradation.

Table 2. Boundary conditions adopted in the thermal transient analysis

Boundary Conditions	***Value***
Input Power	800 W/cm^2
Sink Temperature	50°C
Surface film condition h	5 $W/m^2\ K$

Table 3. Material properties used for the simulation of the ablation tests

Property	***Value***	***Source***
Virgin Mass Density ρ_v	1385 kg/m^3	Experimental test
Degraded Mass Density ρ_d	1218 kg/m^3	Experimental test
Virgin Specific Heat C_v	880 $J/kg \cdot K$	Experimental test
Degraded Specific Heat C_d	1820 $J/kg \cdot K$	Experimental test
Virgin Out-of-Plane Thermal Conductivity k_v^{OOP}	0.43 $W/m \cdot K$	Experimental test
Degraded Out-of-Plane Thermal Conductivity k_d^{OOP}	0.5 $W/m \cdot K$	Arnold et Al. [3]
Virgin In-Plane Thermal Conductivity k_v^{IP}	3 $W/m \cdot K$	Arnold et Al. [3]
Degraded In-Plane Thermal Conductivity k_d^{IP}	1 $W/m \cdot K$	Arnold et Al. [3]
Degradation Heat	-293 kJ/kg	Sykes [40]
Thermal Emissivity ε	0.8	Machado et Al. [41]

A first thermal transient analysis was run with these parameters, then a campaign of analyses was run changing the parameter one by one to understand its influence on the overall results. These parameters were tuned within the ranges reported in Table 4.

Table 4. Tuning ranges of most influent parameters

Property	***Minimum Value***	***Maximum Value***
Virgin In-Plane Thermal Conductivity k_v	3 $W/m \cdot K$	10 $W/m \cdot K$
Degraded In-Plane Thermal Conductivity k_d	0.8 $W/m \cdot K$	1.2 $W/m \cdot K$

Degraded Out-of-Plane Thermal Conductivity k_d	$0.3\ W/m \cdot K$	$1\ W/m \cdot K$
Boundary Condition Sink Temperature	$30°C$	$70°C$
Thermocouples Position (longitudinal)	$-1\ mm$	$+1\ mm$

The results of this tuning campaign are shown in Figure 11, where the experimental temperature curves are compared with the data obtained by the numerical simulations.

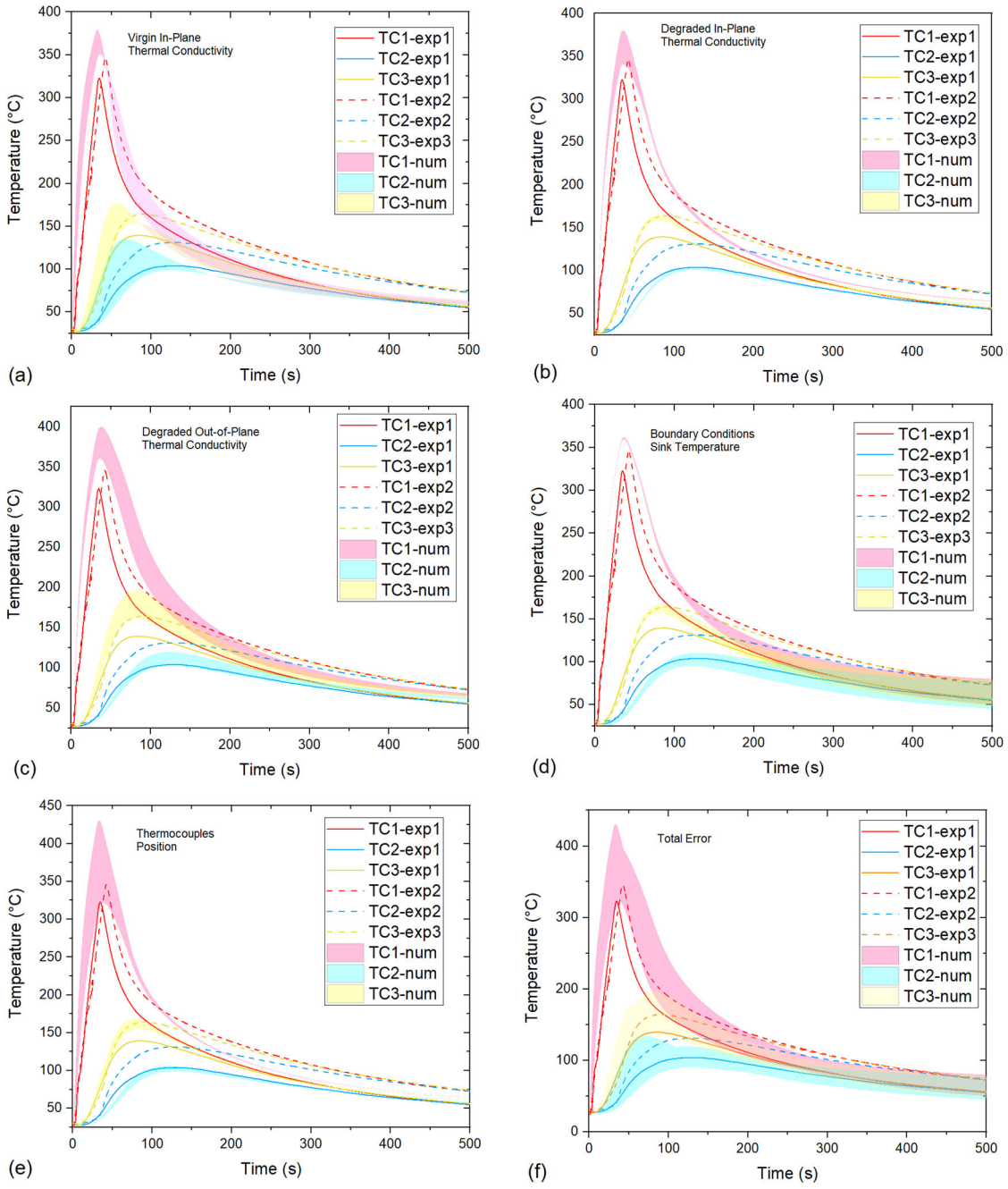

Figure 11. Tuning of thermal simulation parameters (see table 4): (a) virgin In-Plane thermal conductivity, (b) degraded In-Plane thermal conductivity, (c) degraded Out-of-Plane thermal conductivity, (d) boundary conditions sink temperature, (e)

thermocouples position, (f) combined effects i.e. maximum error of simulated temperature given the tuned parameter.

These data are reported as bands ranging between minimum and maximum value of the tuning range. Five elements affecting the temperature were considered: (a) the virgin In-Plane thermal conductivity, (b) the degraded In-Plane thermal conductivity, (c) the degraded Out-of-Plane thermal conductivity, (d) the boundary conditions sink temperature, (e) the thermocouples position to take into account the manufacturing errors. In Figure 11-f the sum of all five elements of errors is considered to evidence the maximum band of difference as compared to the experimental temperature profiles.

In Figure 12, the section cut of the simulated geometry is shown, in the area where the torch is applied. It shows the temperatures map at 0, 10, 20, and 30 seconds after the torch shutdown, in a simulation run with the parameter reported in Table 3.

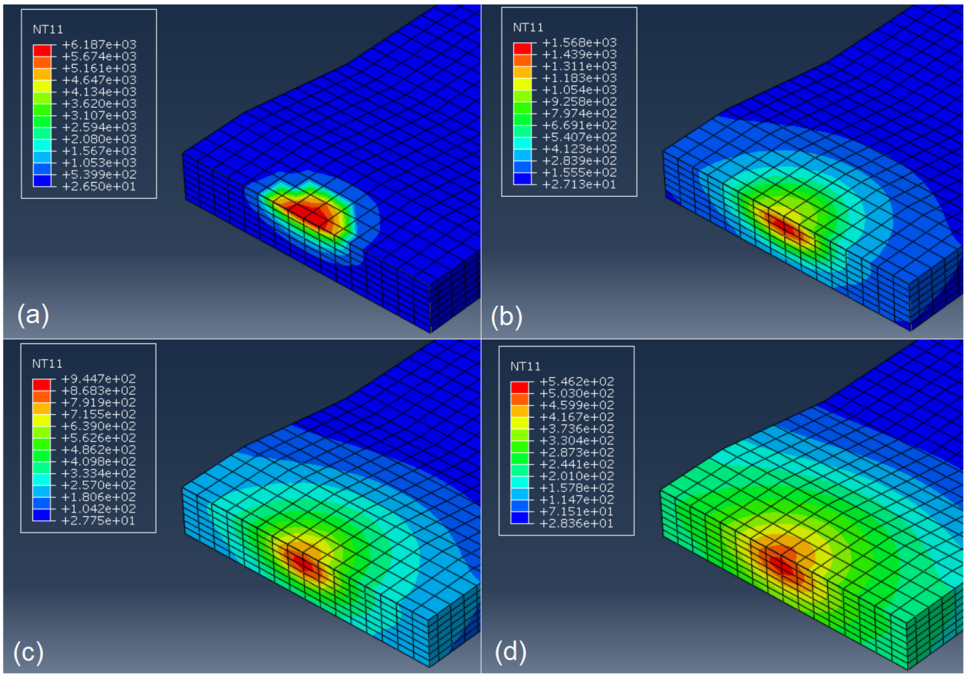

Figure 12. (a) Map of simulated temperature in °C, at the torch shutdown in correspondence of the torch application point, (b) 10 seconds after the torch shutdown, (c) 20 seconds after the torch shutdown, (d) 30 seconds after the torch shutdown.

These results show that there is a good correspondence between the real and the simulated material, thus providing a validation for the proposed approach based on finite element analysis and the material subroutine presented in Section 4.3.

5. Correlation between temperature experienced and residual strength

As the CPC layers in contact with the hot gases are subjected to degradation reactions, the internal layers should maintain adequate stiffness and strength to perform structural roles. The specimens designed for the OAT tests and the numerical reconstruction of temperature maps make possible a correlation between the temperature reached in the different zones of the specimens and the residual mechanical properties.

5.1 Four Points Bending tests

Three tapered specimens were subjected to a Four Points Bending (FPB) test. Two of them were previously subjected to OAT test as described in Section 4. The FPB causes in a tapered specimen the arising of a state of stress with strong out-of-plane components in the tapering zone [36-39]. Indeed, the specimens were designed with the aim of obtaining an interlaminar failure in such a zone. The tests were conducted by using the same 810 MTS apparatus which was set for an imposed displacement rate of 1 mm/min. The specimens were placed onto 15 mm diameter cylindric supports as shown in the Figure 13, with a span between the upper ones of 112 mm and of 260 mm between the lower ones. The failure mode, shown in Figure 13, was characterized by the development of delamination starting for the end of the tapered zone and propagating towards the thin central part of the specimen.

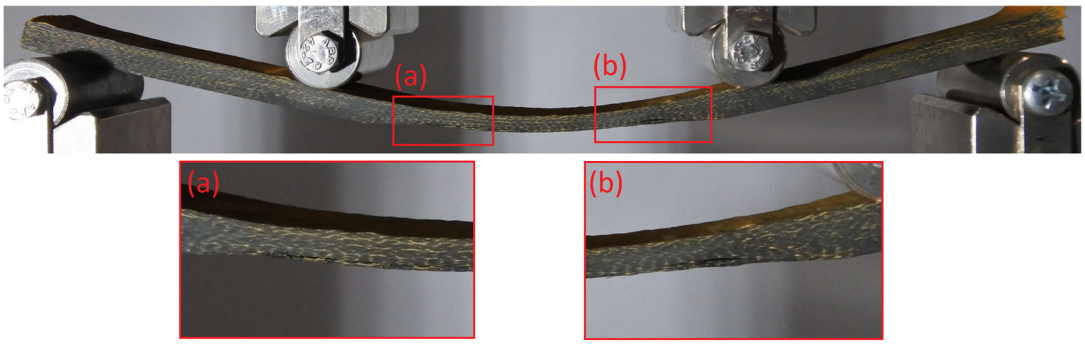

Figure 13. Failure of a specimen subjected to FPB with a focus on the delaminated areas.

The force vs. displacement curves are presented in Figure 14 for one as-built specimen and two specimens subjected to OAT. Sample 2 and Sample 3, the degraded specimens, show a deviation from the linear response starting from an absolute value of the force equal to about 1.2 kN, with a series of load drops that did not lead immediately to a catastrophic failure, which occurred at about 1.50 kN These discontinuities in the curves could be related to the development of delamination cracks at the end of the tapered zone. Final failure actually occurred on the compressed side for Sample 2, while Sample 3 experienced an unstable propagation of the delamination damage. Sample 1, the virgin specimen, exhibited a linear response until 1.75 kN and failed by sudden propagation of delamination at both end of the tapered zones.

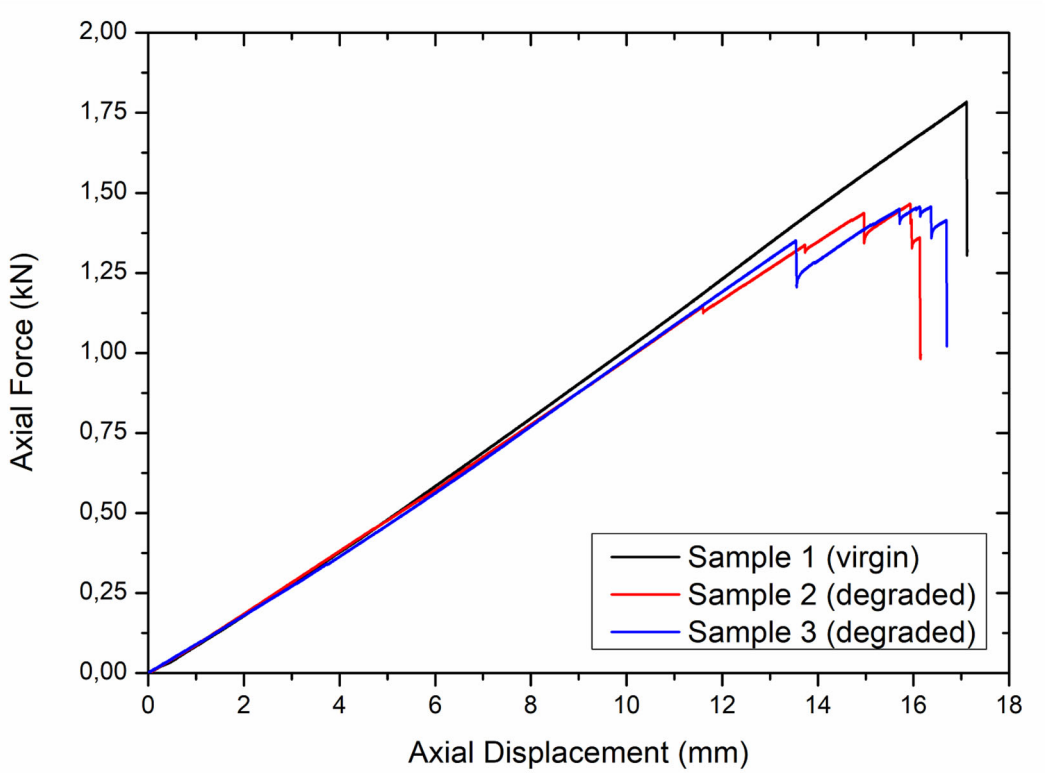

Figure 14. Comparison between FPB curves of virgin and degraded specimens.

The temperature map provided in Figure 12, was taken in correspondence of the maximum temperature at the end of the tapered zone, which resulted of about 120°C. Therefore, the results obtained with the FPB tests on tapered specimens indicated the possibility of a reduction of interlaminar strength above 200°C.

5.2 Short Beam Test

Two SBT series were tested, the first batch on specimens of the as-built material and the second set on coupons obtained by cutting samples (slices) from a FPB specimen subjected to OAT. They were cut transversally from the thick part of a tapered coupon, as explained in Section 4.1 (see Figure 6-b). The tests were performed using ASTM D2344 Standard [42] as a guide. In other words, five as-built CPC specimens were cut from a laminate with a $[0]_{28}$ lay-up, while five samples were cut from a degraded FPB specimen starting from the point of application of the torch and progressively moving towards the end. In this way, each specimen of this series experienced a progressively decreasing maximum temperature, which was evaluated by using the map made available by the

numerical results, as shown in Figure 12. The average thickness and width were 7.02 ± 0.06 mm and 12.53 ± 0.49 mm, respectively, while the length was 40 mm. The MTS 810 system was set for a displacement-controlled test at a displacement rate of 0.5 mm/min. In each one of the specimens, failure occurred with a series of sequential delaminations in the zone between the loading nose and one of the supports. The delamination sequence typically followed an inclined pattern, as shown in Figure 15-a. The force vs. displacement response was repeatable for all the as-built specimens, as presented in Figure 15-b. Curves of degraded specimens deviate monotonically from the as-built ones.

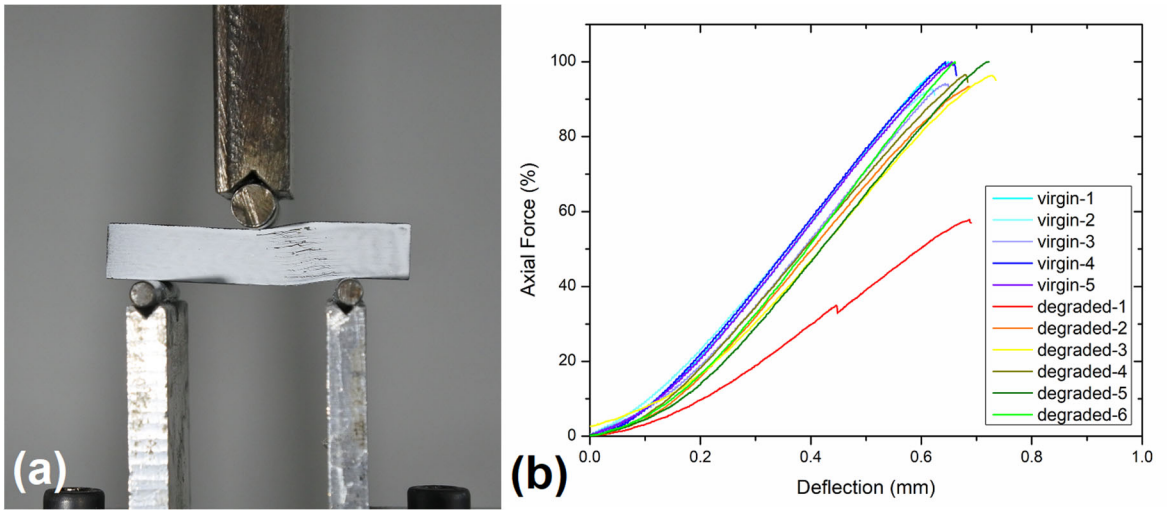

Figure 15. SBT tests: (a) Typical failure during a SBT test; (b) load/ deflection curves.

From force-displacement curves, the ILSS value was obtained through Eq. 2 [42]:

$$ILSS = 0.75 \times \frac{P}{t \times w} \quad (2)$$

Where P is the axial load, t and w are the specimen thickness and width, respectively. From a quantitative point of view, the values of the ILSS obtained on the samples of the first set of coupons were in line with the results typically referred CPCs produced with ex-PAN CFs [1, 13, 35]. Such results indicate that in the cases in which the OOA process did not exhibited technical problems during the manufacturing, the technique adopted did not have a detrimental effect on the interlaminar strength and represent, together with the results obtained in the DCB tests, a

promising indication of the level of interlaminar mechanical properties that can be achieved through vacuum infusion.

The curve shown in Figure 16-a presents the percentage of residual ILSS retained by the specimens as a function of the maximum temperature extrapolated from the numerical model, in the two points shown in Figure 16-b. The curves were normalized with respect to the maximum strength recorded among all the tests. These curves were then compared with the data elaborated from the values published in [1]. It can be observed that until 100°C no significant reduction of interlaminar strength was evaluated to the material produced in this work. Data indicate that a small reduction can occur between 100°C and 200 °C, whereas the strength is likely to be significantly reduced between 200°C and 400°C, consistently with the results of FPB test. The trend is in qualitative agreement with the corresponding presented in [1], which was obtained by conditioning the CPC specimens with a hot furnace.

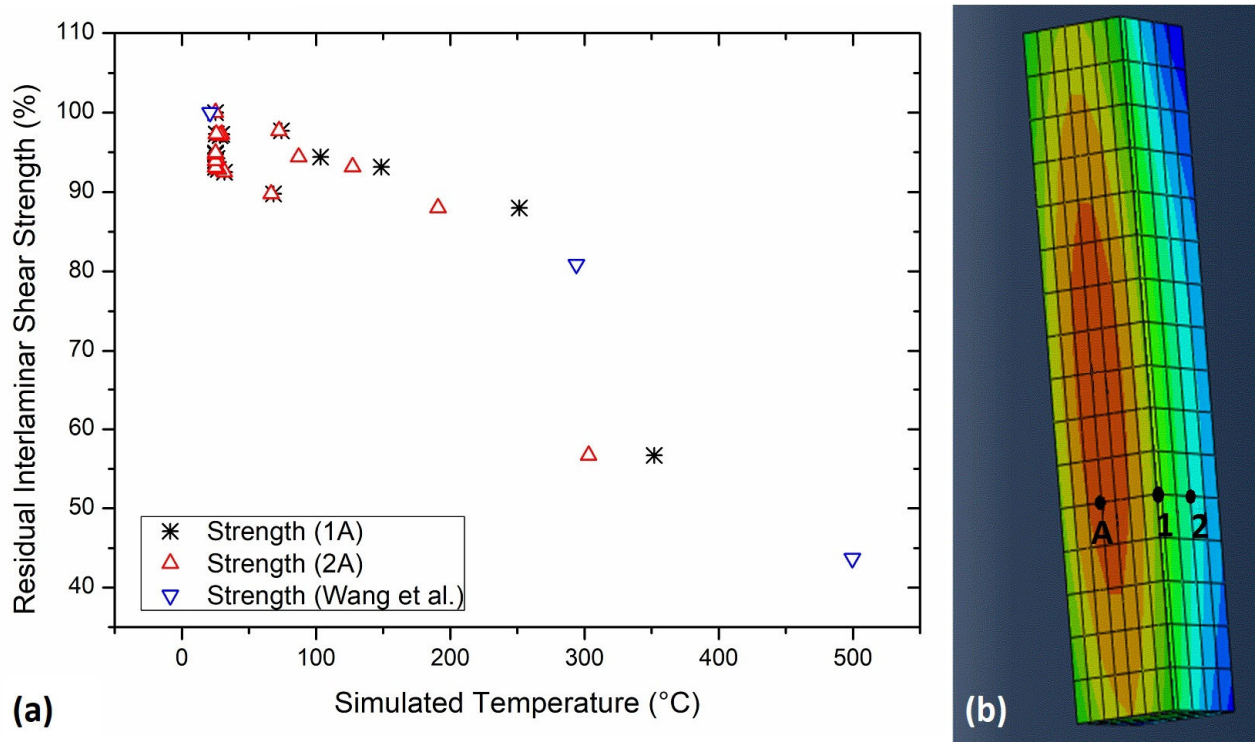

Figure 16. Correlation between experimentally measured residual ILSS with numerically simulated temperature: (a) ILSS vs. Simulated Temperature in 1A and 2A compared with literature, (b) 1A and 2A points definition [1].

6. Conclusions

In this work Carbon/Phenolic Composites (CPCs) made using Out-Of-Autoclave (OOA) processes were produced. The Double Bag Vacuum Infusion (DBVI) process did not exhibit technical problems during the manufacturing, the technique adopted did not have a detrimental effect on the matrix-dominated in-plane properties of the CPCs. As a result, in some scenarios, DBVI process technique to produce some specific CPC parts could promote a certain reduction of the manufacturing time and cost. CPC laminates produced in this way were characterized and they showed adequate properties to play a structural role. Specimens with more complex geometry were designed to investigate the correlation between thermal and mechanical properties using a network of embedded sensors. Considering the data acquired from test and sensors, a thermal simulation of the OAT ablation test was setup and validated. The modelling approach, based on a subroutine linked to Simulia/Abaqus code, proved to be capable to estimate with a good approximation the profile of temperatures into the structural layers of the specimen during the test. The relationship between experimentally measured mechanical properties and the temperature, simulated by the model tuned with the experimental data, shows a good agreement with literature [1]

The model was used to evaluate the temperature experienced in different zones of the specimens during the ablation tests and to correlate them with the degradation of the properties measured in subsequent mechanical tests. Results shows that 90% of the interlaminar strength of the as-built material is maintained after the exposure of temperature up to 200 °C, thus indicating that the internal layer of the CPC laminate produced may perform reliable structural roles even if subjected to extreme temperature on the surface. The numerical-experimental protocol constituted by the integration of the thermal numerical model, the ablation tests, and the mechanical tests performed on specifically designed specimens, represent a promising procedure for the design of the CPC components exposed to harsh environments.

7. Acknowledgement

This work was conducted within project COMETAS (Cost Effective Material and Technologies for Access to Space) funded under the H2020-MANUNET (Ref. MNET17/NMCS-1177) initiative.

8. References

[1] T. Wang, C. Zhou, Y. Ju and X. Chen, "Mechanical Properties with High Temperature and the Microstructure of Carbon/Phenolic Ablative Composites" *Journal of Wuhan University of Technology-Mater,* vol. 27, p. 967–972, 2012.

[2] M. Satyanarayana Gupta and J. Ekta, "Review on Evaluation of properties of carbon phenolic composite structure using gas chromatography for analysis of thermal performance" in *IOP Conference Series: Materials Science and Engineering*, Telangana, India,

2018.
[3] S. M. Arnold, P. L. Murthy, B. A. Bednarcyk, J. W. Lawson, J. D. Monk and C. W. J. Bauschlicher, "Multiscale Modeling of Carbon/Phenolic Composite Thermal Protection Materials: Atomistic to Effective Properties" NASA, NASA Glenn Research Center Cleveland, OH United States, 2016.
[4] M. Natali, J. Kenny and L. Torre, "Science and technology of polymeric ablative materials for thermal protection systems and propulsion devices: A review" *Progress in Material Science,* vol. 84, pp. 192-275, 2016.
[5] H. L. N. Mcmanus and G. S. Springer, "High Temperature Thermochemical Behavior of Carbon-Phenolic and Carbon-Carbon Composites, I. Analysis" *Journal of Composite Materials,* vol. 26, p. 206, 1992.
[6] D. Bianchi, A. Turchi, F. Nasuti and M. Onofri, "Chemical Erosion of Carbon-Phenolic Rocket Nozzles" *Journal of Propulsion and Power,* vol. 29, no. 5, pp. 1220-1230, 2013.
[7] J. Haiyun, W. Jigang, W. Shenquing, Y. Zhiqing, H. Zhongliang, W. Ruomei and L. Qilong, "The pyrolysis mechanism of phenol formaldehyde resin" *Polymer Degradation and Stability,* vol. 97, no. 8, pp. 1527-1533, 2012.
[8] A. C. Cortopassi, "Erosion of carbon-cloth phenolic nozzles in rocket motors with aluminized solid propellant," UMI Dissertation Publishing, 2012.
[9] A. C. Cortopassi, E. Boyer, R. Acharya and K. K. Kuo, "Design of a Solid Rocket Motor for Characterization of Submerged Nozzle Erosion" in *44th AIAA/ASME/SAE/ASEE Joint Propulsion Conference & Exhibit*, Hartford, CT, 2008.
[10] S. Shilds, "Scout Nozzle Data Book," NASA, 1975.
[11] R. Lee, "Interlaminar Factors in Rayon vs. PAN-Based Laminate Composites" Huntsville, AL: NASA Marshall Space Flight Center, 2010
[12] D. Anqi, Z. Yan, Z. Xinqing and Y. Qiyong, "Cure Cycle Optimization of Rapidly Cured Out-Of-Autoclave Composites," *MDPI Materials,* vol. 11, no. 3, p. 421, 2018.
[13] J. Sha, J. Dai, J. Li, Z. Wei and K. W. Hausherr J.M., "Measurement and analysis of fiber-matrix interface strength of carbon fiber-reinforced phenolic resin matrix composites" *Journal of Composite Materials,* vol. 48, no. 11, pp. 1303-1311, 2014.
[14] B. Y. Lattimer, J. Ouellette and J. Trelles, "Thermal Response of Composite Materials" *Fire Technology,* vol. 47, no. 4, p. 823–850., 2011.
[15] J. Henderson, J. Wiebelt and M. Tant, "A Model for the Thermal Response of Polymer Composite Materials with Experimental Verification" *Journal of Composite Materials,* vol. 19, p. 579, 1985.
[16] A. Mouritz, S. Feih, E. Kandare, Z. Mathys, A. Gibson, P. Des Jardin, S. Case and B. Lattimer, "Review of fire structural modelling of polymer composites" *Composite: Part A,* vol. 40, p. 1800–1814, 2009.
[17] A. Mouritz, Z. Mathys and A. Gibson, "Heat release of polymer composites in fire" *Composite: Part A,* vol. 37, p. 1040–1054, 2006.
[18] B. Yu, V. Till and K. Thomas, "Modeling of thermo-physical properties for FRP composites under elevated and high temperature" *Composites Science and Technology,* vol. 67, pp. 3098-3109, 2007.
[19] T. M. Vetter, J. Bibinger, F. E. S. Zimmer and H.-J. Gudladt, "Characterization of one-sided thermal damage of carbon fiber reinforced polymers by means of depth profiles" *Journal of Composite Material,* vol. 54, no. 24, p. 3699–3713, 2020.
[20] L. Torre, J. M. Kenny and A. M. Maffezzoli, "Degradation behaviour of a composite material for thermal protection systems Part I–Experimental characterization" *Journal of Material Science,* vol. 33, pp. 3137-3143, 1998.
[21] L. Torre, J. M. Kenny and A. M. Maffezzoli, "Degradation behaviour of a composite material for thermal protection systems. Part II - process simulation." *Journal of Material Science,* vol. 33, pp. 3145-3149, 1998.
[22] L. Torre, J. M. Kenny, G. Boghetich and M. A. M., "Degradation behaviour of a composite material for thermal protection systems. Part III - char characterization" *Journal of Material Science,* vol. 35, pp. 4563-4566, 2000.
[23] M. Natali, I. Puri, J. M. Kenny, L. Torre and M. Rallini, "Microstructure and ablation behaviour of an affordable and reliable nanostructured Phenolic Impregnated Carbon Ablator (PICA)" *Polymer Degradation and Stability,* vol. 141, pp. 84-96, 2017.
[24] T. Hou and B. J. Jensen, "Evaluation of Double-Vacuum-Bag Process for Composite Fabrication" NASA Langley Research Center, 2004.
[25] "Standard Test Method for Mode I Interlaminar Fracture Toughness of Unidirectional

Fiber-Reinforced Polymer Matrix Composites" ASTM International, West Conshohocken (PA), US, 2013.
[26] "Standard Test Method for In-Plane Shear Response of Polymer Matrix Composite Materials by Tensile Test of a 45° Laminate," ASTM International, West Conshohocken (PA), US, 2018.
[27] S. Ghiasvand, A.Airoldi, P.Bettini, C.Mirani, " Analysis of residual stresses and interface damage propagation in hybrid composite/metallic elements monitored through optical fiber sensors" *Aerospace Science and Technology*, In Press, https://doi.org/10.1016/j.ast.2022.107373
[28] C.S. Lopes, P.P. Camanho, Z. Gürdal, P. Maimí, E.V. González, "Low velocity impact damage on dispersed stacking sequence laminates. Part II: Numerical simulations" *Composites Science and Technology*, Vol. 69, no. 7-8, pp. 937-947, 2009
[29] J. K. Park, D. Cho, T. J. Kang, "A comparison of the interfacial, thermal, and ablative properties between spun and filament yarn type carbon fabric/phenolic composites" *Carbon, Vol 42, no.4, pp. 795-804, 2004*
[30] Lee, R. "Fiber Surface Treatments and Matrix Interface Effects." Huntsville, AL: NASA Marshall Space Flight Center, 2009
[31] Lee, R. "Interlaminar Strengthening Concepts for Polymer Matrix Composites - A Survey of New and Improved Techniques for Advancing the State-Of the Art in Composite Design and Manufacturing." Huntsville, AL: NASA Marshall Space Flight Center, 2014
[32] M. Natali, M. Rallini, L. Torre, D. Puglia, "High Temperature Composites From Renewable Resources: A Perspective on Current Technological Challenges for the Manufacturing of Non-Oil Based High Char Yield Matrices and Carbon Fibers" *Polymeric and Composite Materials*, 2022
[33] A. Paul, J. G. P. Binner, B. Vaidhyanathan, A. C. J. Heaton & P. M. Brown, "Heat flux mapping of oxyacetylene flames and their use to characterise Cf-HfB2 composites" *Advances in Applied Ceramics*, Vol. 115, no. 3, pp. 158-165, 2016
[34] "Standard Test Method for Measuring Heat-Transfer Rate Using a Thermal Capacitance (Slug) Calorimeter" ASTM International, West Conshohocken, PA, 2020, 2020.
[35] I. Abramovitch, N. Hoter, H. Levy, A. Gedanken, A. Wolf, A. Eitan, T. Fine, L. Elmaleh, I. Shalev, G. Cohen, E. Grimberg, Y. Nevo and O. Shoseyov, "Effects of the 3D sizing of polyacrylonitrile fabric with carbon nanotube–SP1 protein complex on the interfacial properties of polyacrylonitrile/phenolic composites" Journal of Composite Materials, vol. 50, p. 1031–1036, 2016.
[36] A. Airoldi, G. Sala, P. Bettini and A. Baldi, "An efficient approach for modeling interlaminar damage in composite laminates with explicit finite element codes" *Journal of Reinforced Plastics and Composites,* vol. 32, no. 15, p. 1075–1091, 2013.
[37] S. Giannis, "Utilising fracture mechanics principles for predicting the mixed-mode delamination onset and growth in tapered composite laminates" *Composite Structures,* vol. 102, pp. 294-305, 2013.
[38] J. C. Fish and S. W. Lee, "Delamination of Tapered Composite Structures" *Engineering Fracture Mechanics,* vol. 34, no. 1, pp. 43-54, 1989.
[39] K. He, S. Hoa and R. Ganesan, "The study of tapered laminated composite structures: a review" *Composites Science and Technology,* vol. 60, pp. 2643-2657, 2000.
[40] G. F. J. Sykes, "Decomposition characteristics of a char-forming phenolic polymer used for ablative composites" NASA, NASA Langley Research Center Hampton, VA, United States, 1967.
[41] H. A. Machado, P. G. Silva Pesci and C. Paterniani, "Effect of the atmosphere in the ablation of Carbon-Phenolic Composites used in Thermal Protection Systems" in *BCCM4 - 4th Brazilian Conference on Composite Materials*, Rio de Janeiro, Brazil, 2018.
[42] "Standard Test Method for Short-Beam Strength of Polymer Matrix Composite Materials and Their Laminates" ASTM International, West Conshohocken (PA), US, 2016.